J Mater Sci (2008) 43:6159–6166
DOI 10.1007/s10853-008-2933-2

Formation of nano-columnar amorphous carbon films via electron beam irradiation

Tatsuhiko Aizawa · E. Iwamura · T. Uematsu

Received: 4 June 2008 / Accepted: 5 August 2008 / Published online: 26 August 2008

Abstract Electrical beam (EB) irradiation is used to chemically modify the amorphous carbon film, a-C:H, which is prepared by the DC magnetron sputtering. The starting a-C:H film has vague columnar structure with lower density intercolumns as predicted by Thornton structure model. The EB-irradiated a-C:H film has fine nano-columnar structure with the average columnar size of 10–15 nm. This size is equivalent to the measured in-plain correlation length by the Raman spectroscopy. Little change in the sp2/sp3 bonding ratio is observed in the columnar matrix before and after EB-irradiation. Increase of sp2/sp3 ratio is noted in the intercolumns of irradiated a-C:H films. No change is detected in the hydrogen content of a-C:H films before and after EB-irradiation: 35 at% hydrogen in a-C:H. Increase of the in-plain density via EB-irradiation, is attributed to the increase of local atomic density in the intercolumns, which is measured by the electron energy zero-loss spectroscopy. This local densification is accompanied with ordering or graphitization in the intercolumns of the EB-irradiated a-C:H film. The nano-columnar a-C:H film modified by EB-irradiation has non-linear elasticity where indentation displacement should be reversible up to 8% of film thickness. Owing to this ordering and densification via EB-irradiation, softening both in stiffness and hardness takes place with increasing the irradiation time.

T. Aizawa (✉)
AsiaSEED-Insitute, Tokyo, Japan
e-mail: aizawa@asiaseed.org

T. Aizawa
Japan R&D Laboratory, University of Toronto,
3-15-10, Minami-Rokugo, Ota-City, Tokyo 144-0045, Japan

E. Iwamura
Arakawa Chemical Co. Ltd., 1-1-9 Tsurumi, Osaka 538-0053, Japan

T. Uematsu
Tokyo Metropolitan Industrial Research Institute,
1-20-20, Minami-Kamata, Ota-City, Tokyo 144-0035, Japan

Introduction

Amorphous carbon or Diamond-Like Carbon (DLC) films are wildly used as a protective coating to improve the wear resistance and tribological performance [1]. Various coating methods and procedures have been proposed to lower the residual stresses, to reduce the friction coefficient and to modify their mechanical and functional properties [2, 3]. The variety of amorphous carbon films with the formula of a-C, a-C:H, ta-C, and so forth, is classified for industrial applications by the triangular diagram of sp2 (graphitic bonding state)—sp3 (diamond-state or tetragonal bonding state)–[H] (hydrogen content) [4]. This diagram is effective to identify the targeting area of coating design for each coating procedure. As partially suggested in [5], mechanical properties and response becomes a complex function in these three parameters; e.g., increase of sp3/sp2 ratio in the narrowed [H] zone leads to significant increase of hardness or tribological properties. This classification is true to the single-phase, mono-layered amorphous carbon coatings. However, in the case when a-C:H or a-C films become nano-composite, new design is required not only for classification of coating methods but also for tailored coating design in application [6].

A hybrid system in the amorphous carbon films is popular to make change in their functionality. A hybrid phase of carbons is formed and observed where nano-tubes

and fullerenes are embedded together in the amorphous carbon [7]. This suggests that amorphous carbon films are chemically modified by nano-composite formation in order to improve their mechanical properties and tribological performance. Carbon nanotube is also chemically modified by high-dose electron beam irradiation [8]. This implies that carbon-base structures, once formed, are chemically modified by post-treatment to have a tailored microstructure. Authors have proposed a new methodology of chemical modification for a-C:H films via the low-dose electron beam irradiation [9–12].

In the present article, precise analysis is made to characterize the electron beam irradiation effect on the microstructure of a-C:H film and its properties. The constituent element contents as well as oxygen contaminant concentration are measured by Elastic Recoiling Detection Analysis (ERDA) and Rutherford Back-scattering Spectroscopy (RBS) profiles. Both Transmission Electron Microscopy (TEM) and in-lens Scanning Electron Microscopy (SEM) are used to describe the plan and cross-sectional micrographs of a-C:H film before and after electrical beam (EB)-irradiation. Raman spectroscopy is also used to describe the change of bonding state in a-C:H film and to trace the ordering process via EB-irradiation. In particular, variation of density and bonding state with increasing the irradiation time is discussed with consideration on the change of mechanical properties via EB-irradiation of a-C:H films.

Experimental procedure

Preparation of starting a-C:H films

DC magnetron sputtering with the inter-electrode distance of 100 mm, was used for starting film deposition of amorphous carbon without the bias voltage. The base pressure was 5×10^{-4} Pa. Its power was constant, 500 W. Argon was used as a carrier gas together with hydrogen gas. This mixture gas mass-flow with 95% Ar and 5% H_2, was varied to control the sputtering pressure (P). Silicon substrate with $10 \times 10 \times 0.5$ mm^3 was utilized for microstructure analysis and observation. The starting amorphous carbon film with a-C:H was prepared by $P = 1.4$ Pa. The film thickness (t) was constant, $t = 1$ μm for TEM observation of initial a-C:H film and $t = 250$ nm for EB-irradiation.

Electron beam irradiation

Mini-EB (Ushio, Inc.) was used for low-energy electron beam (EB) irradiation. Its accelerated voltage and current were 60 kV and 0.3 mA, respectively. Its dose rate was fixed only 6.0×10^{11} s^{-1} mm^{-2}. This dose is much lower in the order of 10^{-6} to 10^{-7} than that in TEM observation. Since the displacement atoms (dpa) are estimated to be dpa $\ll 10^{-6}$, there is no physical effect on the irradiation of a-C:H films [9]. Furthermore, since the maximum temperature rise is limited by 450 K [10], there might be little possibility of hydrogen dissociation from a-C:H films to be discussed later.

Microstructure analysis

Transmission Electron Microscopy and High Resolution TEM (HRTEM) was utilized for precise observation of microstructure. In-lens SEM by Hitachi S-4800 with the resolution of 1 nm, was also used to make surface and cross-sectional observation of a-C:H films before and after EB-irradiation. Using the electron zero-loss energy spectrum in the energy-filtered HRTEM, both atomic and electron densities were estimated in local.

Raman spectroscopy was used to describe the change of bonding state before and after EB-irradiation. In general, the Raman spectrum of a-C:H films has two peaks: G-peak corresponding to graphite peak at higher wave number of C–C bonding, and, D-peak, to disorder-induced peak at its lower wave number. Integrated peak intensity ratio of I(D)/I(G) for these two peaks, often becomes a parameter not only to describe sp2–sp3 bonding state change in a-C:H film but also to estimate the nanostructure size. In particular, after Tuinstra–Koenig relation [13], the in-plain correlation length (La) is estimated from this ratio: e.g., I(D)/I(G) is proportional to $(La)^2$ for the disordered amorphous carbon films.

ERDA and RBS

Elastic Recoiling Detection Analysis and RBS were utilized to describe the variation of element contents (especially carbon and hydrogen) before and after EB-irradiation and to estimate the in-plain atomic density. He^+ beam with 2.3 MeV was used for analyses. The current is limited by 30 nA. Both the element concentration and the in-plain atomic density are estimated by the area ratios in ERDA and RBS profiles.

Mechanical characterization

Nano-indention system (ENT-1100a) with the Berkovich-type diamond indentor, was used for mechanical characterization. Indentation depth is controlled to be less than 1/10 of film thickness in order to eliminate the substrate effect on the measured load-displacement curve or W-δ curve. From the measured W-δ curve, both the equivalent Young's modulus (E) and hardness (H) are obtained by the following equations:

$$E = \pi^{1/2} / \left[2A^{1/2}(d\delta/dW)_{Wmax}\right], \quad (1)$$

$$H = Wmax / A, \quad (2)$$

where A is the true projective contact area of indentor, and, Wmax, the maximum indentation load.

Experimental results

Characterization of initial a-C:H films

Figure 1 shows the plan and cross-sectional views of as-deposited a-C:H film by TEM. After the Thorson structural model for three dimensional growth of amorphous carbon [14], this film is characterized by a vague, naturally growing columnar nano-structure. This columnar structure has 20–40 nm in diameter and lower density intercolumns. After [10, 11], this column diameter (D) is related to the film thickness (t) because of low thermal mobility and shadowing effect in natural evolution of film structure. Since $(D/0.1) = t^{0.8}/3$, D at $t = 1$ μm is estimated to be 0.034 μm.

This a-C:H is also characterized by its Raman spectrum. As depicted in Fig. 2, the measured Raman spectrum has two peaks: G-peak at around 1,550 cm^{-1} and D-peak at around 1,400 cm^{-1}, respectively. From the integrated intensity ratio of these two peaks, the in-plain correlation length is estimated, La = 1 nm from I(D)/I(G) = 1.511. That is, this initial a-C:H film mainly has disordered amorphous state without any ordered nanostructure in it.

Characterization of EB-irradiated a-C:H films

In-lens SEM is used for microstructure observation of irradiated samples. Figure 3 depicts both the plan and cross-sectional views of irradiated a-C:H films after EB-irradiation for 3.6 ks. This irradiated film is characterized by fine, columnar structure in the depth of film. The average diameter of each column ranges 10–15 nm. Comparing the plan views before and after irradiation in Figs. 1 and 3, the surface roughness is nearly the same between two; no change occurs in surface roughness by irradiation. Most difference in microstructure before and after irradiation lies in the fact that fine columnar structure is formed to have distinct inter-columns in a-C:H matrix with vertical alignment in the depth.

This change in microstructure reflects on the bonding state of a-C:H. Figure 4 shows the Raman spectrum of irradiated sample together with the best-fitted peak profiles. This spectrum is characterized by four peak profiles or two pairs of D/G peak profiles. Table 1 summarizes peak position for D- and G-peaks, their Full Width Half Maximum

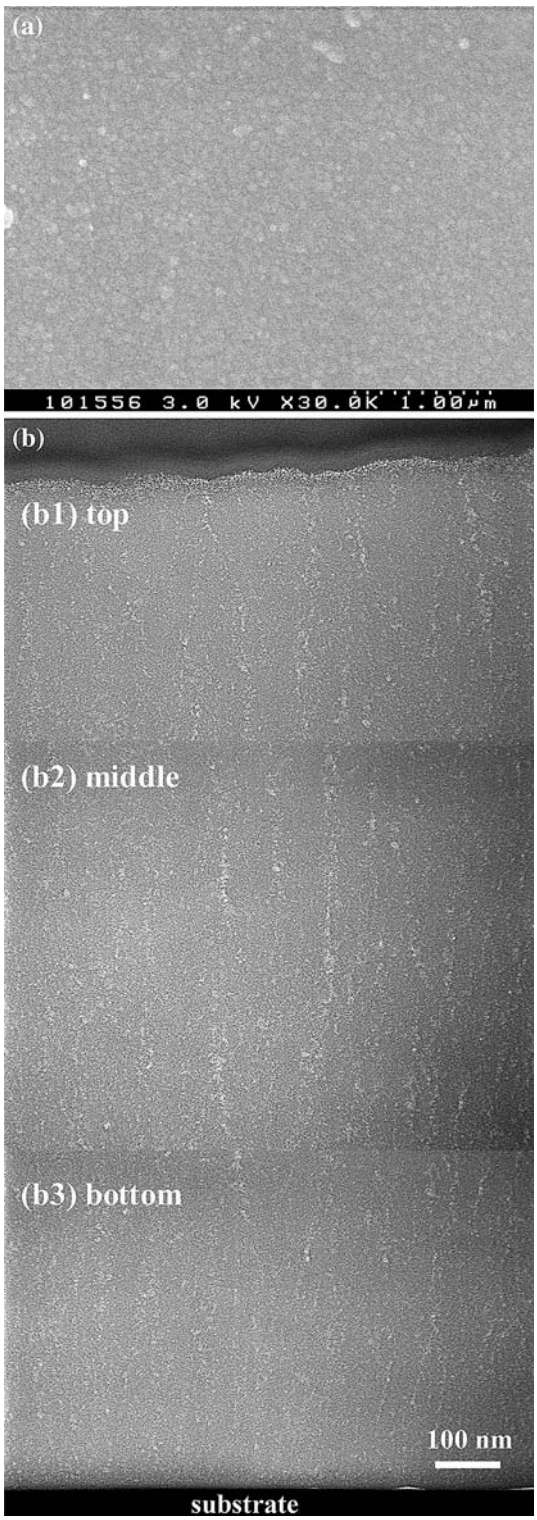

Fig. 1 TEM image of starting a-C:H films: (**a**) Plan view and (**b**) Cross-sectional view

(FWHM) and integrated intensity ratio I(D)/I(G) both for as-deposited and irradiated samples. In Fig. 4, D1 and G1 peaks correspond to original a-C:H film in Fig. 2. The positions of D- and G-peaks in Fig. 2, are ω_D = 1,385.6

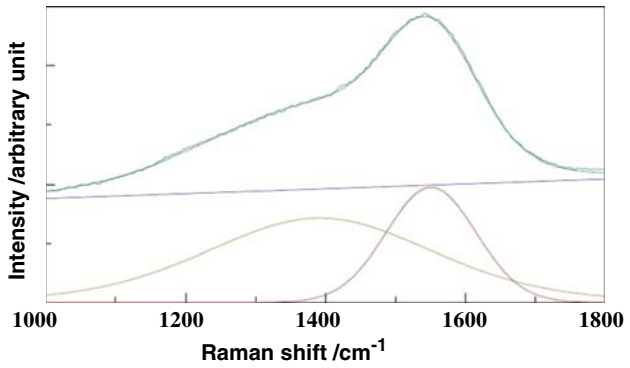

Fig. 2 Raman spectrum of starting a-C:H films with the best-fitted profiles

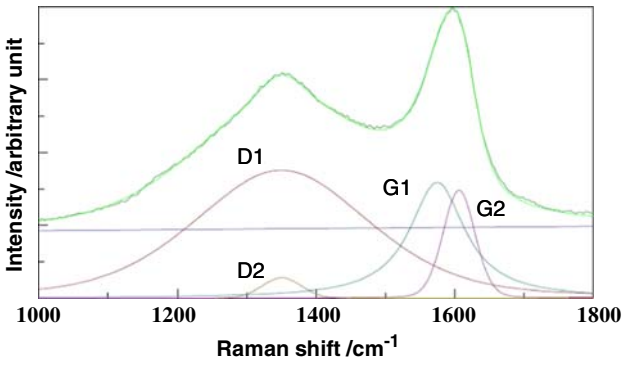

Fig. 4 Raman spectrum of EB-irradiated a-C:H films with the best-fitted profiles

cm^{-1}, $\phi_D = 357.9\ cm^{-1}$ and $\omega_G = 1{,}551.1\ cm^{-1}$, $\phi_G = 154.5\ cm^{-1}$, respectively before EB-irradiation. While in Fig. 4, $\omega_{D1} = 1{,}354.3\ cm^{-1}$, $\phi_{D1} = 316.3\ cm^{-1}$ and $\omega_{G1} = 1{,}577.4\ cm^{-1}$, $\phi_{G1} = 91.7\ cm^{-1}$, respectively after EB-irradiation. Hence, $\omega_{D1} \approx \omega_D$, and, $\omega_{G1} \approx \omega_G$, respectively. In addition, from I(D1)/I(G1) = 2.321, La is estimated to be around 2 nm. Since both D/G peak positions and La are nearly coincident with each other, the columnar matrix in the irradiated a-C:H film has the same disordered C–C bonding state as before irradiation.

New D2 and G2 peaks appear in Fig. 4 together with original D1 and G1 peaks. This implies that new phase could be formed in the original a-C:H columnar matrix. After Tuinstra–Koenig relation for graphitic structure [13], I(D2)/I(G2) is proportional to $(La)^{-2}$. Since I(D2)/I(G2) = 0.636, La is estimated to be La = 10 nm. This in-plain correlation length is nearly equal to the average diameter of columns in Fig. 3. Then, these new D2/G2 peaks are characteristic to the irradiated intercolumns.

Change of microstructure, composition, and properties

Together with sp2 and sp3 bonding state, hydrogen content affects the microstructure and bonding state of a-C:H films. ERDA is used to quantitatively estimate the hydrogen content in a-C:H films before and after EB-irradiation. In order to prove the sensitivity of ERDA to change of hydrogen content, the sputtering pressure was varied from original condition, $P = 1.4$ Pa, to reference condition, $P = 0.2$ Pa. Figure 5 shows the ERDA profiles for as-deposited samples at $P = 1.4$ and 0.2 Pa, respectively and for an irradiated sample which was deposited at $P = 1.4$ Pa. In using the DC magnetron sputtering process, the hydrogen content in the deposited a-C:H films is thought to reduce drastically with decreasing the sputtering pressure [6]. In fact, the measured ERDA profile area for $P = 0.2$ Pa, is much smaller than that for $P = 1.4$ Pa. This proves that ERDA is a suitable tool to describe hydrogen content change in a-C:H films during EB-irradiation. Figure 5 directly demonstrates that no change occurs in the hydrogen content before and after EB-irradiation: hydrogen content is constant, [H] = 35% in Table 2. Hence, the change of microstructure and bonding state observed by EB-irradiation has nothing to do with hydrogen content.

Together with ERDA, RBS is also utilized to detect other elements even in the trace level and to measure their contents both in the as-deposited and irradiated a-C:H films. As shown in Fig. 6, oxygen content is noted as a contaminant located near carbon in the RBS spectrum. Since both profiles for oxygen and carbon significantly overlap on each other, actual contaminant level is much smaller than seen in Fig. 6. From the area ratio for each element both in ERDA and RBS profiles, atomic concentration of elements as well as in-plain atomic density are

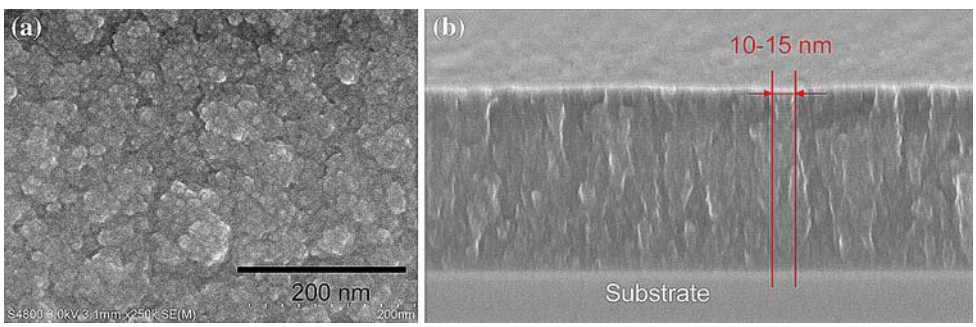

Fig. 3 In-lens SEM image of EB-irradiated a-C:H films: (**a**) Plan view and (**b**) Cross-sectional view

Table 1 Variation of G and D peak positions, their FWHM and G/D-peak integrated intensity ratio with increasing the irradiation time (t)

Sample	D-peak		G-peak		I(D)/I(G)
	Position ω_D (cm^{-1})	FWHM ϕ_D (cm^{-1})	Position ω_G (cm^{-1})	FWHM ϕ_G (cm^{-1})	
First D/G peak					
a-C:H at $t = 0$ s	1385.6	357.9	1551.1	154.5	1.511
a-C:H at $t = 300$ s	1364.7	323.5	1562.1	114.1	2.295
a-C:H at $t = 3{,}600$ s	1354.3	316.3	1577.4	91.7	2.321
Second D/G peak					
a-C:H at $t = 0$ s	–	–	–	–	–
a-C:H at $t = 300$ s	1356.7	94.3	1601.0	70.27	0.419
a-C:H at $t = 3{,}600$ s	1349.5	84.2	1606.8	54.8	0.636

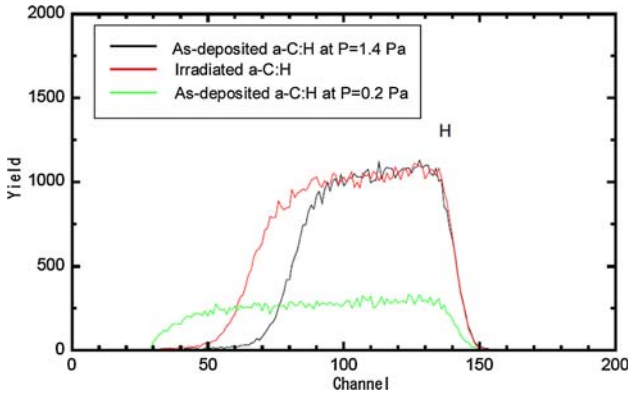

Fig. 5 Comparison of ERDA profiles for hydrogen in the starting a-C:H films prepared at $P = 1.4$ Pa and $P = 0.2$ Pa, and, in the EB-irradiated a-C:H film

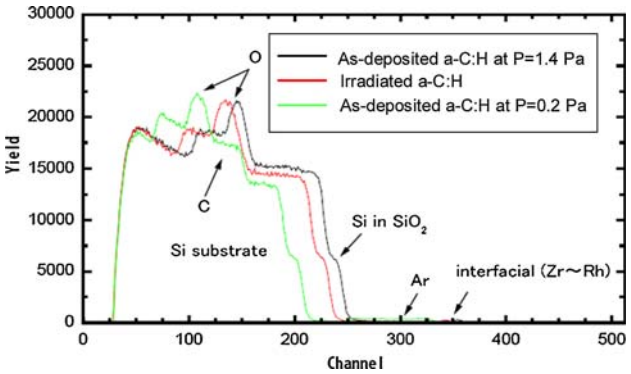

Fig. 6 Comparison of various element concentrations detected by RBS in the starting a-C:H films prepared at $P = 1.4$ Pa and $P = 0.2$ Pa and in the EB-irradiated a-C:H film

estimated. Table 2 lists the calculated concentration of hydrogen, oxygen, and carbon with the in-plain atomic density both for as-deposited and irradiated samples. The average atomic density increases via EB-irradiation by 25%.

Figure 7 compares the plan view of as-deposited and irradiated a-C:H films by using the energy-filtered HRTEM with the threshold energy of 25 eV. In this micrograph, the black image corresponds to lower density phase while the light image, to higher density phase. As depicted in Fig. 7a, the initial as-deposited a-C:H has an intercolumn with lower density than inside of columns. After EB-irradiation, this density distribution is modified to the situation where the intercolumn has higher density than inside of columns, as shown in Fig. 7b. Table 3 lists the atomic density estimated for columns and intercolumns both in the as-deposited and irradiated a-C:H films. Local increase of atomic density at the intercolumns, corresponds to average increase of atomic density by 25%.

Effect of EB-irradiation time on the change of properties for a-C:H films

EB-irradiation time is varied to describe the effect of irradiation time (t) on the change of properties described in the above. Figure 8 compares the Raman spectra at $t = 0$, 300 s and 3,600 s, respectively. The measured Raman spectra at $t = 300$ s and 3,600 s are nearly the same. This proves that the change of microstructure in the inter-columnar region advances during short duration time in EB-irradiation. In-lens SEM was used to describe this

Table 2 Comparison in the detected hydrogen, oxygen and carbon concentrations and the in-plain atomic density by ERDA and RBS analysis, before and after EB-irradiation

Sample	O-content (%)	H-content (%)	C-content (%)	Atomic density (atoms/m^2)
As-deposited sample at $P = 1.4$ Pa	4.1 ± 2	36.3 ± 2	59.6 ± 2	4.06×10^{22}
Irradiated sample	1.8 ± 2	35.0 ± 2	63.2 ± 2	5.09×10^{22}

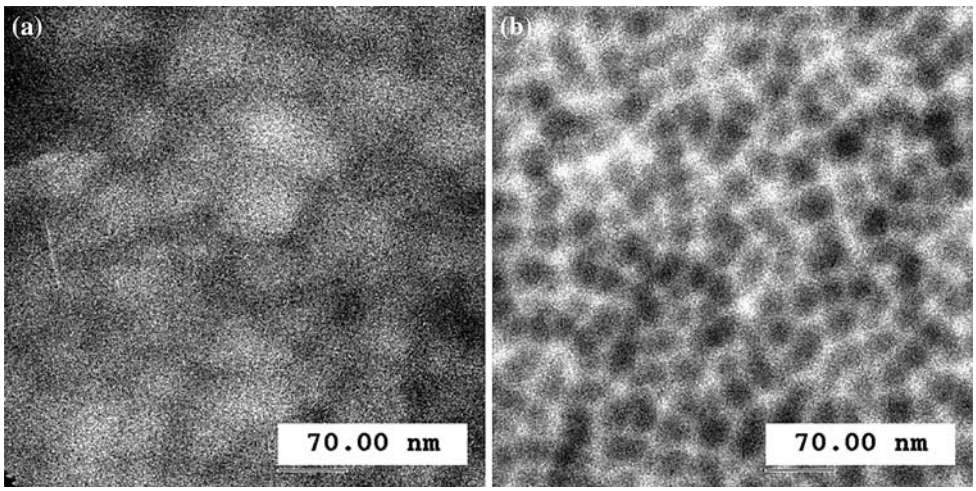

Fig. 7 Comparison of energy-filtered HRTEM image for surface of samples before and after EB-irradiation: (**a**) Before EB-irradiation and (**b**) After EB-irradiation

Table 3 Change of local atomic density in the column matrix and intercolumns via EB-irradiation

Sample	Column	Inter-columnar region
As-deposited sample at $P = 1.4$ Pa	1.8 Mg/m^3	1.6 Mg/m^3
Irradiated sample	1.8 Mg/m^3	>1.9 Mg/m^3

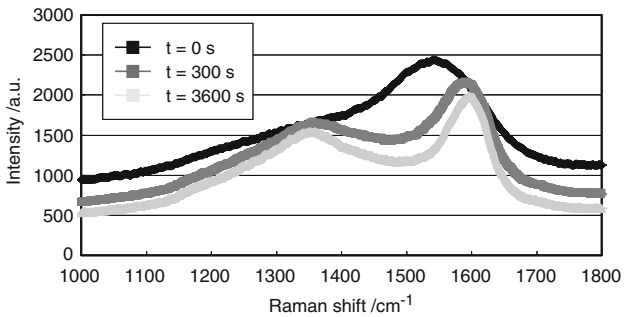

Fig. 8 Variation of Raman spectrum for a-C:H films with increasing the irradiation time (t)

variation of microstructure with increasing the EB-irradiation time. As shown in Fig. 9, finer columnar structure is noted even when $t = 300$ s. Comparing SEM-micrographs at $t = 300$ s and 3,600 s, much finer nano-columnar structure is observed with increasing the irradiation time.

Figure 10 depicts the variation of load-displacement curves with increasing the irradiation time. In the as-deposited a-C:H film, large hysteresis between loading and unloading curves is noticed; plastic straining and cracking might occur in the film during loading and unloading. In the irradiated a-C:H films at $t = 300$ s and 3,600 s, this hysteresis is significantly much reduced within an intrinsic error of tolerance in the present nano-indention mechanism. That is, the irradiated a-C:H film has non-linear elasticity where load-displacement curve becomes reversible up to 8% of film thickness. Although the non-dimensional load-displacement curve or (W/W_{max})–(δ/δ_{max}) is nearly the same between $t = 300$ s and 3,600 s, the maximum displacement (δ_{max}) increases itself at the same load limit (W_{max}) with increasing the irradiation time. This softening behavior of mechanical properties is described by decrease of Young's modulus and hardness with t. As shown in Table 4, E and H decrease monotonically with t and converge to the stationary values; i.e., E = 60 GPa and H = 10 GPa.

Discussion

No change of hydrogen content in a-C:H films is observed during EB-irradiation by ERDA and RBS measurements. The densification detected by RBS is attributed to increase of number of carbon atoms per unit volume in a-C:H film by EB-irradiation. As listed in Table 3, no significant increase of local atomic density in the columns is measured by electron zero-loss energy spectrum in the energy-filtered HRTEM. The above densification detected by ERDA and RBS is attributed to the selective increase of carbon atomic density in the intercolumns. No change of hydrogen content via EB-irradiation also assures that the temperature rise during EB-irradiation is never enough to make hydrogen dessociation. The onset temperature of dissociation for hydrogen atoms from a-C:H is about 623 K. Authors had concluded in the previous papers [9, 10] that no change was noticed in the Raman spectrum even after long-term heat treatment of initial a-C:H films up to 753 K. Hence, the microstructure change in the intercolumns driven by EB-irradiation has nothing to do with direct annealing effect [15].

In the Raman spectroscopy, first D/G peak positions are nearly the same before and after EB-irradiation. This implies that columnar matrix in the irradiated a-C:H films has the same bonding state as before irradiation. No change

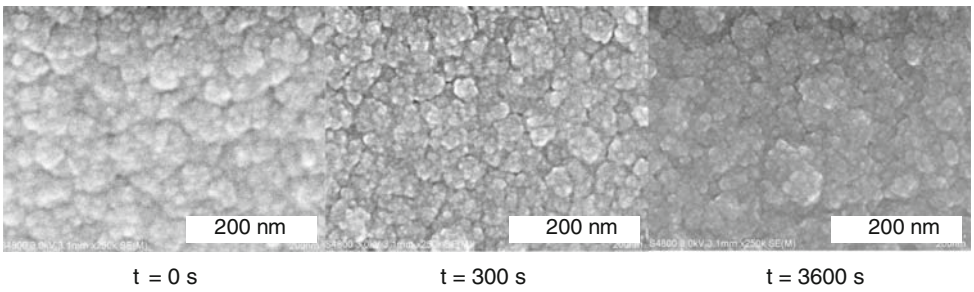

Fig. 9 Variation of plan view in the in-lens SEM-micrographs for a-C:H films with increasing the irradiation time (*t*)

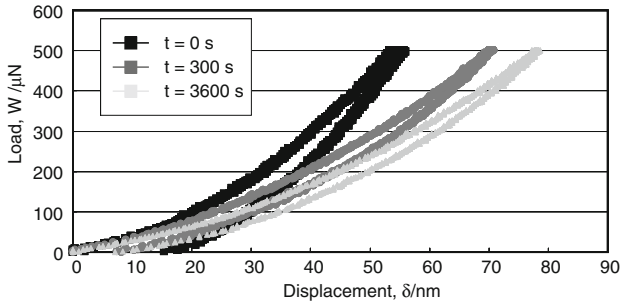

Fig. 10 Variation of load-displacement curves obtained by nano-indentation test with increasing the irradiation time (*t*)

Table 4 Variation of Young's modulus (E), maximum hardness (H) and elastic hardness (He) with increasing the irradiation time

Sample	Young's modulus, E (GPa)	Maximum hardness, H (GPa)	Elastic hardness, He (GPa)
a-C:H at $t = 0$ s	130	24	6.7
a-C:H at $t = 300$ s	73	13	3.8
a-C:H at $t = 3{,}600$ s	61	10.5	3.2

of density and in-plane correlation length in columnar matrix also proves the fact that columnar matrix has the same disordered state as before irradiation. That is, the columnar matrix is not chemically modified. New G/D peaks with high intensity for G-peak appear in the Raman spectrum of irradiated a-C:H films. This proves that an ordering process or a graphitization takes place during EB-irradiation. Since the in-plain correlation length estimated from this peak ratio is equivalent to the columnar size in microstructure, this graphitization advances selectively in the intercolumns. Hence, selective graphitization in the intercolumns accompanies with densification in themselves via EB-irradiation. Initial a-C:H film has a vague columnar structure where relatively high-density a-C:H columns is covered by lower density intercolumns with the same sp2–sp3 bonding and hydrogen content. After EB-irradiation, high-density inter-columnar network with higher sp2/sp3 bonding ratio is embedded into the original a-C:H matrix, having the same sp2/sp3 bonding ratio and hydrogen content as the as-deposited a-C:H film.

Vertical alignment of graphitized intercolumns in the a-C:H matrix reflects on the mechanical response in nano-indentation. Non-linear elasticity in nano-indentation up to 8% of film thickness, is a unique characteristic to this vertically aligned nano-composite a-C:H film. This originates from the mechanical response of vertically aligned high-density network embedded in disordered a-C:H matrix; further precise analysis and theoretic modeling is needed to explain the relationship between this nano-composite structure and reversible mechanical response. In particular, softening or hardening behavior might be controlled by this nano-composite structure.

In the following, the softening process with decrease of Young's modulus and hardness via EB-irradiation is discussed by nano-composite modeling for this vertical alignment of graphitized intercolumns in the disordered a-C:H matrix.

Since the initial a-C:H film has E = 130 GPa and H = 24 GPa, the a-C:H matrix after EB-irradiation also has the same Young's modulus and hardness; i.e., the Young's modulus of matrix (E_m) is 130 GPa. In this nano-composite, a graphitic phase with lower elastic stiffness (E_g) is vertically aligned with the volume fraction of f in the above disordered amorphous carbon matrix with E_m. Then, according to the classical composite theory [16], the Young's modulus of this nano-composite film (E_{com}) is represented by the following equation:

$$1/E_{com} = (1 - f)/E_m + f/E_g. \quad (3)$$

The volume fraction f is geometrically estimated from Figs. 3 and 7 by assuming that a regular hexagonal prism column with the diameter D has a peripheral intercolumnar layer with the thickness of d. Then, f is simply calculated by

$$f = 1 - (1 - d/D)^2. \quad (4)$$

D is around 10–15 nm, and, d, at most 0.5 nm. Hence, f = 6–9%. Since $E_{com} = 60$ GPa, E_g is estimated from Eq. 3 to be 6.4–9.3 GPa. References [17, 18] reported that sp2-bonded high-quality pure graphite has the Young's modulus of 5–10 GPa. This agreement implies that softening process is selected by this nano-composite formation, where a pure graphitic intercolumn is vertically aligned with the volume fraction of 6–9% in the disordered a-C:H matrix.

Conclusion

Amorphous carbon film was prepared by the DC magnetron sputtering to have the naturally growing vague columnar structure and the hydrogen content of 35%. This film is further subjected to EB-irradiation for its chemical modification. No change in hydrogen content occurs before and after EB-irradiation. Owing to this irradiation, the ordering process takes place in the intercolumns as a graphitization from low-density amorphous carbon to higher density phase. After this ordering with densification, the initial a-C:H film is chemically modified to have nano-composite structure with a vertically aligned graphitic network in the disordered state amorphous carbon matrix. This formation of nano-composite film reflects on its mechanical properties and response. Since the loading and unloading curves in the nano-indentation tests are overlapped in nearly perfect up to 8% of film thickness, this film has non-linear elasticity. Reduction of stiffness and hardness or softening with irradiation time is accompanied with graphitization in the intercolumns.

Acknowledgement Authors would like to express their gratitude to Mr. T. Fukuda and Mr. H. Morishita, R & D center, Mitsue Die and Mold Co. Ltd. for experimental help in use of Raman spectroscopy.

References

1. Kim KY et al (1996) Surf Coat Technol 87:569. doi:10.1016/S0257-8972(96)02966-0
2. Vercammen K et al (2000) Surf Coat Technol 134:466. doi:10.1016/S0257-8972(00)00925-7
3. Dai L (ed) (2006) Carbon nanotechnology. Elsevier, New York
4. Ferrari AC, Robertson J (2000) Phys Rev B 61:14095. doi:10.1103/PhysRevB.61.14095
5. Bewilogua K et al (2008) Abstract ICMCTF-2008 (San Diego), p 67
6. Suzuki H, Ikenaga M (2003) Applications of DLC coating. Nikkan-Kougyou Shinbun
7. Chhowalla M et al (1997) Philos Mag Lett 75:329. doi:10.1080/095008397179598
8. Gupta S et al (2006) Mater Sci 21:3109
9. Iwamura E (2003) Ceram Trans 148:139
10. Iwamura E (2003) Rev Adv Mater Sci 5:34
11. Iwamura E, Aizawa T (2006) Mater Res Soc Symp Proc 908E:0011-05
12. Aizawa T, Iwamura E, Itoh K (2007) Surf Coal Technol 202:1177
13. Tuinstra F, Koenig JL (1970) J Comp Mater 4:492
14. Thornton JA (1974) J Vac Sci Technol 11:666
15. Chung CK, Wun BH (2006) Thin Solid Films 515:1985. doi:10.1016/j.tsf.2006.08.012
16. Mura T (1987) Micromechanics of defects in solids, 2nd edn. Martinus Nijhoff Publishing, Dordrecht
17. http://www.tanso.org/search/index. Accessed 27 May 2008
18. http://www.poco.com. Accessed 28 May 2008